Preprint
UCRL-JC-134169

Validation of Numerical Shallow Water Models for Tidal Lagoons

D.E. Eliason and A.J. Bourgeois

This article was submitted to
American Society of Civil Engineers 6th International Conference on
Estuarine and Coastal Modeling
New Orleans, LA
November 3-5, 1999

November 1, 1999

U.S. Department of Energy
Lawrence
Livermore
National
Laboratory

VALIDATION OF NUMERICAL SHALLOW WATER MODELS FOR TIDAL LAGOONS

by

Donald E. Eliason
Atmospheric Science Division, L-103
Lawrence Livermore National Laboratory
P.O. Box 808, Livermore, CA 94551-9900
Phone: 925 423-5625, Fax: 925 422-6388

and

Alfred J. Bourgeois
US EPA MD-24/ERC-1B
Research Triangle Park, NC 27711

November 1999

ABSTRACT

An analytical solution is presented for the case of a stratified, tidally forced lagoon. This solution, especially its energetics, is useful for the validation of numerical shallow water models under stratified, tidally forced conditions. The utility of the analytical solution for validation is demonstrated for a simple finite difference numerical model. A comparison is presented of the energetics of the numerical and analytical solutions in terms of the convergence of model results to the analytical solution with increasing spatial and temporal resolution.

INTRODUCTION

Validation of coastal and estuarine hydrodynamic models suffers from a paucity of multi-dimensional analytical solutions that include both barotropic and baroclinic effects. The purpose of the present study is to provide one such analytical solution and its energetics. It is a two-dimensional (length, depth), time-dependent solution of both the barotropic and baroclinic modes of a tidally forced lagoon. It extends the work of Eliason and Bourgeois (1997, hereinafter EB97) to the forced case.

In addition to presenting the analytical solution for a stratified tidal lagoon, the validation of a simple finite difference numerical model is presented as an example. An open boundary condition (OBC) has to be used for the tidally forced end of the lagoon. The treatment of open boundary conditions (OBCs) has been given much attention in the literature. In particular, the recent study by Shulman *et al.* (1999, hereinafter SLM99) summarizes the literature on the subject with regard to problems of geophysical interest. The present analytical solution will be shown to validate a non-optimized version of the OBC given by SLM99.

GOVERNING EQUATIONS

As for the unforced case of seiche motions considered by EB97, if one uses the Boussinesq, hydrostatic, and incompressible assumptions, and neglects the nonlinear terms in the momentum equation and the horizontal advection of density in the density equation, the equations of motion that are applicable to tidally forced motion in a Cartesian coordinate, two-dimensional (length, depth) channel can be simplified to:

$$\frac{\partial u}{\partial t} + \frac{1}{\rho_0}\frac{\partial P}{\partial x} = 0 \tag{1}$$

$$\frac{\partial u}{\partial x} + \frac{\partial w}{\partial z} = 0 \tag{2}$$

$$\frac{\partial P}{\partial z} + \rho g = 0 \tag{3}$$

$$\frac{\partial \rho}{\partial t} + w\frac{\partial \rho}{\partial z} = 0 \tag{4}$$

Here u and w are velocity components in the respective x (length) and z (depth, positive upward) directions; t is time; g is the Earth's gravitational acceleration; P is the hydrostatic pressure; and ρ and ρ_0 are the water density and reference water density, respectively.

Barotropic and Baroclinic Modes

Following EB97, we decompose Eqs. 1–4 into depth-averaged and depth-variable components, which correspond to the barotropic and baroclinic modes, respectively. The pressure, P, is first decomposed into a surface pressure, $\rho_0 g\eta$ (where η is the perturbation of the surface from mean sea level) and an internal pressure, p. The surface pressure corresponds to the barotropic mode, and the internal pressure corresponds to the baroclinic mode. The barotropic mode equations are then:

$$\frac{\partial \bar{u}}{\partial t} + g\frac{\partial \eta}{\partial x} = 0 \tag{5}$$

$$\frac{\partial \eta}{\partial t} + H\frac{\partial \bar{u}}{\partial x} = 0 \tag{6}$$

$$\frac{\partial \bar{u}}{\partial x} + \frac{\partial \bar{w}}{\partial z} = 0 \tag{7}$$

where $\bar{u}$ and $\bar{w}$ are the barotropic horizontal and vertical speeds, respectively; and H is the bottom depth.

The corresponding baroclinic equations, for which the density advection term has been linearized, are (EB97):

$$\frac{\partial u'}{\partial t} + \frac{1}{\rho_0}\frac{\partial p'}{\partial x} = 0 \tag{8}$$

$$\frac{\partial u'}{\partial x} + \frac{\partial w'}{\partial z} = 0 \tag{9}$$

$$\frac{\partial p'}{\partial z} + \rho' g = 0 \tag{10}$$

$$\frac{\partial \rho'}{\partial t} + w'\frac{\partial \bar{\rho}}{\partial z} = 0 \tag{11}$$

where u' and w' are the baroclinic horizontal and vertical speeds. The perturbation density, ρ', is a perturbation about a linear background vertical profile of density, $\bar{\rho} = \rho_0 - z\Delta\bar{\rho}$. The internal pressure, p, is correpondingly decomposed into a constant background vertical profile $\bar{p}$, about which the internal perturbation pressure, p', is perturbed, subject to the constraint that $\int_{-H}^{0} p'\,dz = 0$.

Boundary Conditions

For a tidal channel the boundary conditions for the barotropic equations (5–7) are

$$\begin{aligned} \bar{u} &= 0 && \text{at } x = 0, \lambda; \\ \eta &= \eta_T \cos \omega_0 t && \text{at } x = 0, \lambda; \\ \bar{w} &= \partial \eta / \partial t && \text{at } z = 0, \text{ and} \\ \bar{w} &= 0 && \text{at } z = -H, \end{aligned}$$

where $x = 0$ to λ represents one tidal wavelength, $\lambda = c_0 T$, with c_0 the gravity wave speed $c_0^2 = gH$ and T the tidal period; η_T is the tidal amplitude and ω_0 is the tidal frequency, $2\pi/T$; $z = 0$ is at mean sea level and the flat bottom is at $z = -H$.

The tidal channel boundary conditions for the baroclinic equations (8–11) are

$$\begin{aligned} u' &= 0 \quad \text{at } x = 0, \lambda; \\ w' &= 0 \quad \text{at } z = -H, 0; \text{ and} \\ \rho' &= 0 \quad \text{at } z = -H, 0. \end{aligned}$$

ANALYTICAL SOLUTION

The barotropic equations (5–7), subject to the tidal channel boundary conditions, are solved by:

$$\eta = \eta_T \cos kx \cos \omega_0 t \tag{12}$$

$$\bar{u} = \frac{c_0 \eta_T}{H} \sin kx \sin \omega_0 t \tag{13}$$

$$\bar{w} = -\frac{\omega_0 \eta_T (z + H)}{H} \cos kx \sin \omega_0 t \tag{14}$$

where $k = 2\pi/\lambda$ is the tidal wavenumber.

The baroclinic set of equations can be combined into one equation for the internal pressure perturbation, $p'_{zztt} = -N^2 p'_{xx}$, where N is the constant background Brunt-Väisälä frequency, $N^2 = -(g/\rho_0)\partial\bar{\rho}/\partial z$. A candidate solution is then $p' = P_m \cos kx \cos(m\pi z/H) \cos \omega t$, where P_m is the amplitude of the internal pressure perturbation of the mth vertical mode. For this solution to be valid, ω is restricted to the set of discrete eigenfrequencies $\omega_m = kNH/(m\pi)$, $m = 1, 2, \ldots$. A complete solution to the baroclinic set of equations (Eq. 8–11), with the tidal channel boundary conditions, is then:

$$u' = u_m \sin kx \cos \frac{m\pi z}{H} \sin \omega_m t \tag{15}$$

$$w' = -\frac{kHu_m}{m\pi} \cos kx \sin \frac{m\pi z}{H} \sin \omega_m t \tag{16}$$

$$p' = P_m \cos kx \cos \frac{m\pi z}{H} \cos \omega_m t \tag{17}$$

$$\rho' = \frac{m\pi P_m}{gH} \cos kx \sin \frac{m\pi z}{H} \cos \omega_m t \tag{18}$$

where $u_m = m\pi P_m/(\rho_0 NH)$ is the amplitude of the mth mode baroclinic horizontal speed.

Energetics

The energetics analysis to be presented here differs from that given by EB97 because of the differences which arise from the fact that the present system is for a forced versus an un-forced system. Because of the forcing the perturbation energy fluxes are treated differently at the boundaries than in EB97. The tidal channel solutions presented above are for a periodic channel. This solution can be applied to the case of a tidal lagoon by considering the nodal point at $x = 0$ to be instead the closed end of the lagoon. The mouth of the lagoon at $x = L < \lambda$ is forced by the tide. It is this tidal forcing that gives rise to non-zero perturbation energy fluxes at the mouth of the lagoon that distinguishes energetics analysis of the present study from that presented in EB97.

The beginning of the energetics analysis, the total perturbation energy balance equation for the barotropic mode, is the same as in EB97; that is,

$$\frac{d\bar{E}}{dt} + \bar{F}(x=0,t) + \bar{F}(x=L,t) = 0 \tag{19}$$

where $\bar{E}$ is the total barotropic perturbation energy per unit length, and $\bar{F}(x=0,t)$ and $\bar{F}(x=L,t)$ are the barotropic perturbation energy fluxes at the ends of the lagoon. $\bar{E}$ is composed of the barotropic kinetic and available potential perturbation energies, $\overline{KE}$ and $\overline{APE}$ respectively:

$$\begin{aligned} \bar{E} &= \int_0^L \left(\frac{1}{2}\rho_0 H\bar{u}^2 + \frac{1}{2}\rho_0 g\eta^2\right) dx \\ &= \overline{KE} + \overline{APE}. \end{aligned} \tag{20}$$

As in the closed basin, unforced case considered by EB97, the barotropic perturbation energy flux $\bar{F}(x,t) = \rho_0 gH\bar{u}\eta$ is zero at the closed end of the lagoon due to the boundary conditions. In contrast, $\bar{F}$ is not necessarily zero at the mouth of the tidal lagoon at $x = L$, because it represents the barotropic perturbation energy flux due to the tidal forcing. By applying the barotropic solution for the tidal channel at $x = L$, the barotropic perturbation energy flux at the mouth of the tidal lagoon is found to be

$$\bar{F}(x=L,t) = \frac{\rho_0 g c_0 \eta_T^2}{4} \sin 2kL \sin 2\omega_0 t, \tag{21}$$

which is balanced by the time rate of change of the sum of

$$\overline{KE} = \frac{\rho_0 g \eta_T^2}{4k}(kL - \frac{1}{2}\sin 2kL)\sin^2 \omega_0 t \tag{22}$$

and

$$\overline{APE} = \frac{\rho_0 g \eta_T^2}{4k}(kL + \frac{1}{2}\sin 2kL)\cos^2\omega_0 t. \tag{23}$$

The total barotropic perturbation energy for the tidal lagoon is thus

$$\bar{E} = \frac{\rho_0 g \eta_T^2}{4k}(kL + \frac{1}{2}\sin 2kL\cos 2\omega_0 t). \tag{24}$$

As for the barotropic mode, the total perturbation energy balance equation for the baroclinic mode as given by EB97 pertains here as well:

$$\frac{dE'}{dt} + F'(x=0,t) + F'(x=L,t) + F'(z=-H,t) + F'(z=0,t) = 0, \tag{25}$$

where E' is the total baroclinic perturbation energy per unit length

$$\begin{aligned} E' &= \int_{-H}^{0}\int_{0}^{L}\left(\frac{1}{2}\rho_0 u'^2 + \frac{1}{2}\frac{g^2}{\rho_0 N^2}\rho'^2\right)dx\,dz \\ &= KE' + APE', \end{aligned} \tag{26}$$

with KE' the kinetic and APE' the available potential baroclinic perturbation energies, and the F' are the perturbation energy fluxes through the ends ($\int_{-H}^{0} u'p'\,dz$ at $x = 0, L$) and top and bottom ($\int_0^L w'p'\,dx$ at $z = 0, -H$) of the lagoon.

The boundary conditions for the baroclinic mode of the tidal lagoon make all of the baroclinic perturbation energy fluxes zero except at the mouth of the lagoon, just as for the barotropic mode. The baroclinic perturbation energy flux at the mouth of the lagoon can be found from the tidal channel solution to be

$$F'(x=L,t) = \frac{m\pi P_m^2}{8\rho_0 N}\sin 2kL\sin 2\omega_m t. \tag{27}$$

The kinetic and available potential baroclinic perturbation energies which balance this baroclinic perturbation energy flux through their time rate of change are

$$KE' = \frac{\rho_0 u_0^2 H}{8k}(kL - \frac{1}{2}\sin 2kL)\sin^2\omega_m t \tag{28}$$

and

$$APE' = \frac{\rho_0 u_0^2 H}{8k}(kL + \frac{1}{2}\sin 2kL)\cos^2\omega_m t. \tag{29}$$

The total baroclinic perturbation energy is thus

$$E' = \frac{\rho_0 u_0^2 H}{8k}(kL + \frac{1}{2}\sin 2kL \cos 2\omega_m t). \quad (30)$$

In addition to the integral quantities such as $\bar{E}$ and E' being useful as diagnostics for the numerical solution of tidal lagoons, construction of the energy budget of such a numerical model and comparison with the above analytical solutions is also helpful to ensure that the numerical method only changes the total energy by the influence of the perturbation energy flux at the mouth of the lagoon. Such comparisons with the given analytical solutions are particularly useful for the validation of numerical models of systems like tidal lagoons for which an open boundary condition must be employed. The utility of such a comparison will be demonstrated in the next section.

NUMERICAL MODEL

The simple finite difference numerical scheme to be employed here is basically that of EB97, except that the present scheme includes open boundary conditions (OBCs) at the mouth of the tidal lagoon. The other difference from EB97 is that both the initial condition and the first time-step of the numerical model are taken from the analytical solution, rather than obtaining the first time-step from an explict step.

The OBCs employed in the present study are those of SLM99, except that the present study does not use their optimized form. The OBCs of the present study have the general form

$$uc_m - P/\rho_0 = u_f c_m - P_f/\rho_0, \quad (31)$$

where $c_m, m = 0, 1, \ldots$ are the characteristic velocities of each mode, $c_m^2 = gH_m$, with $m = 0$ corresponding to the barotropic mode with $H_0 = H$, and modes $m = 1, 2, \ldots$ corresponding to baroclinic modes with $H_m = H(\rho_H - \rho_0)/(m^2\pi^2\rho_0)$ the equivalent depths. The separation of the general form of the OBC into barotropic and baroclinic modes is done in an analogous manner to that done for the governing equations (1–4). Details of the exact form of the resulting barotropic and baroclinic OBCs are given in the next two subsections.

Barotropic Mode

The barotropic mode of the numerical model is solved semi-implicitly as in EB97 except that $\bar{u}$ is solved for instead of the transport per unit width used in EB97. Although the spatial and temporal indexing of the finite differences on the Arakawa 'C' grid and the solution of the resulting tridiagonal system is that of EB97, the OBC at the lagoon's mouth changes the computation of the coefficients for the tridiagonal solution at $x = L$, $i = I + 1$. The necessary changes are given in the Appendix.

The barotropic OBC can be obtained from Eq. 31 with $m = 0$ and by recalling that the surface pressure is $\eta/(\rho_0 g)$. It is a non-optimized version of the one given by SLM99 for the barotropic mode:

$$\bar{u}H - c_0\eta = \bar{u}_f H - c_0\eta_f, \tag{32}$$

where $\bar{u}_f$ and η_f are the tidally forced (incoming) barotropic velocity and surface elevation at the mouth of the lagoon. In the present study they will be specified from the tidal channel solution evaluated at $x = L$.

The unforced version of Eq. 32, i.e., the condition that $\bar{u}H = c_0\eta$ at the open boundary, allows waves generated interior to the computational domain to be propagated out along their characteristic. This condition is analogous to propagating outgoing waves out of the open boundary along their characteristic Riemann invariant in gas dynamics, and may be derived using the method of Thompson (1987). In Eq. 32 the outgoing waves which are propagating along their characteristic are balanced by the tidally forced wave which is propagating inward along its characteristic. It has long been used as an OBC for gravity waves following Reid and Bodine (1968), who used Eq. 32 except with $\bar{u}_f = 0$. SLM99 cite Flather (1976) as having introduced the $\bar{u}_f$ term into Eq. 32.

Satisfying Eq. 32 at $x = L$ requires a modification to the standard Thomas algorithm (Thomas, 1949) for solving the tridiagonal system of equations that arises from finite differencing Eqs. 5–6. This modification is given in the Appendix.

Baroclinic Mode

The baroclinic mode finite difference equations are solved by the leapfrog method as given by EB97. The only difference in the numerical solution of the baroclinic mode equations of the present study from that of EB97 is that their free slip boundary condition at $x = L$ required $u'(x = L) = 0$. In contrast, the tidal forcing at $x = L$ in the present study requires that an OBC be imposed upon u'. The OBC imposed in this study upon $u'(x = L)$, which is a non-optimized version of the baroclinic one from SLM99, may be derived from the baroclinic component of Eq. 31:

$$u'c_m - p'/\rho_0 = u'_f c_m - p'_f/\rho_0, \tag{33}$$

which SLM99 point out "... can be interpreted as a special linearization of the Bernoulli equation for each baroclinic mode." In the optimization form of SLM99 the $-c_m$ are Lagrangian mulipliers, of which the average is the group velocity of the mth mode. In the present non-optimized version the c_m are the characteristic velocities of each mode, $c_m^2 = gH_m$.

Application

As in EB97, the numerical model is applied to East Lagoon, a tidal lagoon in Galveston, Texas (Fig. 1). East Lagoon is narrow (maximum cross-channel width 320 m, length

$L = 2\,\mathrm{km}$) and shallow (maximum of $H = 5\,\mathrm{m}$ in depth). The closed end of the lagoon has a summertime stratification that can vary from $\rho_o = 1021\,\mathrm{kg\,m^{-3}}$ at the surface to $\rho_H = 1023\,\mathrm{kg\,m^{-3}}$ at the bottom. Tidal forcing at the open end of the lagoon is primarily due to the M_2 tide ($\bar{T} = 12.42\,\mathrm{hours}$). Using East Lagoon's maximum summertime stratification, the period due to the first baroclinic mode is $T' = 36.7\,\mathrm{days}$.

The base run of the numerical model was done with a a grid size of 128^2 density points, resulting in a spatial resolution of $\Delta x = 15.625\,\mathrm{m}$ and $\Delta z = 3.90625\,\mathrm{cm}$. The duration of this run was T', which will be referred to as a "long" run. A time-step of $\Delta t = T'/4200000 \approx 0.7556\,\mathrm{s}$ was used to ensure that the accuracy requirement of the barotropic mode's tridiagonal solve was met. The accuracy requirement is that $|b_j| \leq |a_j| + |c_j|$, where the $|b_j|$ are the diagonal elements, and the $|a_j|$ and $|c_j|$ are the off-diagonal elements.

To determine the effects of using less resolution, five additional long runs were also made, as summarized in Table 1. Also, one "short" run was done at the 128^2 grid size using $\Delta t = T/60000 = 0.7452\,\mathrm{s}$ to investigate the accuracy of the numerical model's solution of the barotropic mode. As shown in Table 1, the time-steps were varied with spatial resolution to keep the Courant number constant.

Table 1: Grid sizes (number of density points), their corresponding grid interval sizes, and time-steps for the six runs that were done to test the effects of changing resolution.

Grid	$\Delta x\,(\mathrm{m})$	$\Delta z\,(\mathrm{cm})$	$\Delta t\,(\mathrm{s})$
128^2	15.625	3.90625	0.7556532
64^2	31.25	7.8125	1.5113064
32^2	62.5	15.625	3.0226128
16^2	125	31.25	6.0452256
8^2	250	62.5	12.0904512
4^2	500	125	24.1809024

As in EB97, the energetics of the numerical results are compared to the energetics of the analytical solution by computing the root mean square error (RMSE). In contrast to EB97, rather than using the index of agreement (Wilmott, 1981), the percent disagreement, $\%d$, is used for the comparison:

$$\%d = 100\frac{\sum_{n=1}^{n_{max}}(A_n - N_n)^2}{\sum_{n=1}^{n_{max}}(|A'_n| + |N'_n|)^2} \tag{34}$$

where A_n are the analytical energetics (e.g., $\overline{APE}$), N_n are the numerical energetics, $A'_n = A_n - < A >$, and $N'_n = N_n - < A >$, with $< A >$ being the mean of the analytical energetics. Values of $\%d$ which are close to 0 indicate that the model results agree quite well with the

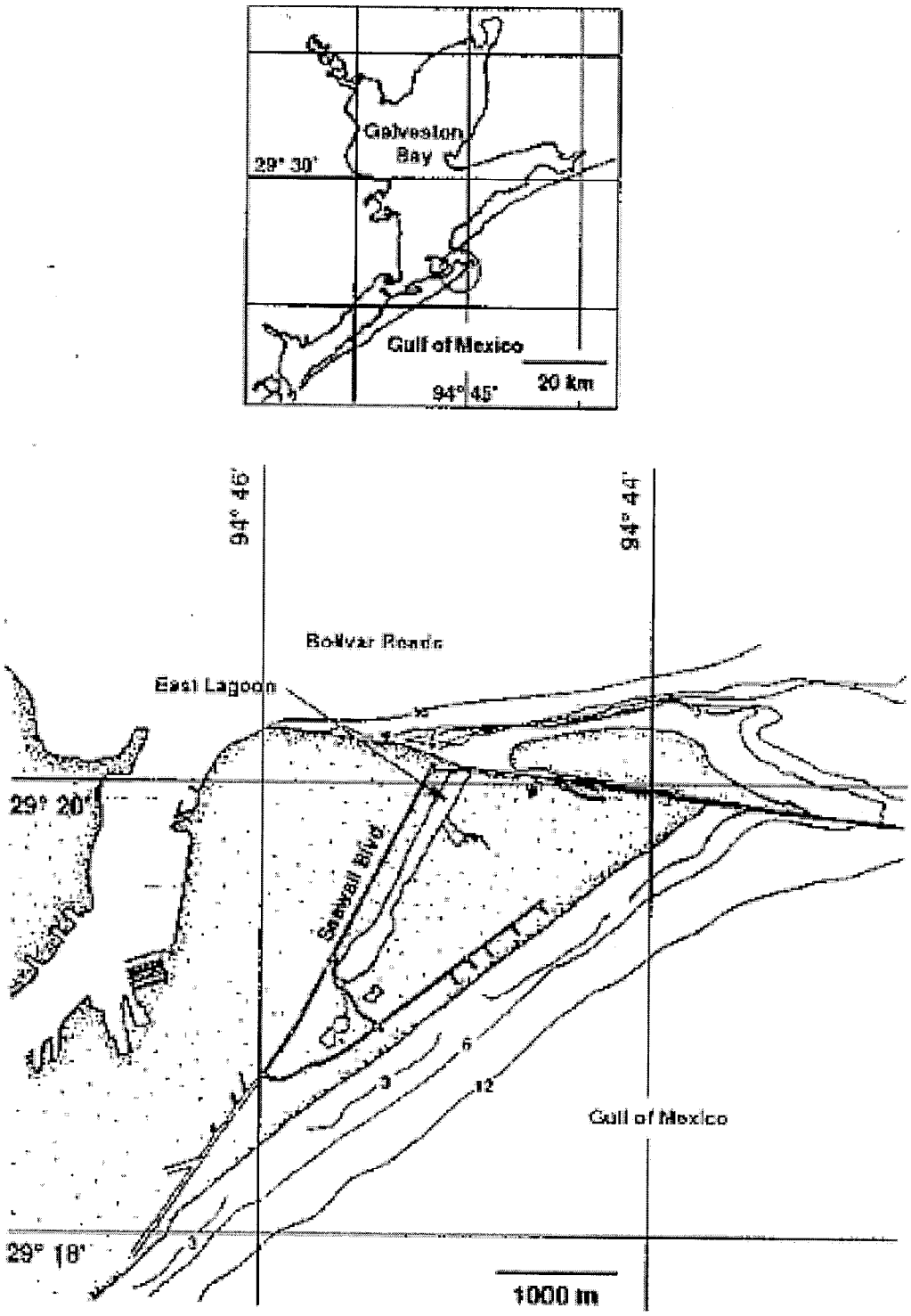

Figure 1: Geographical location of East Lagoon on Galveston Island, Texas (after Livingston, 1981).

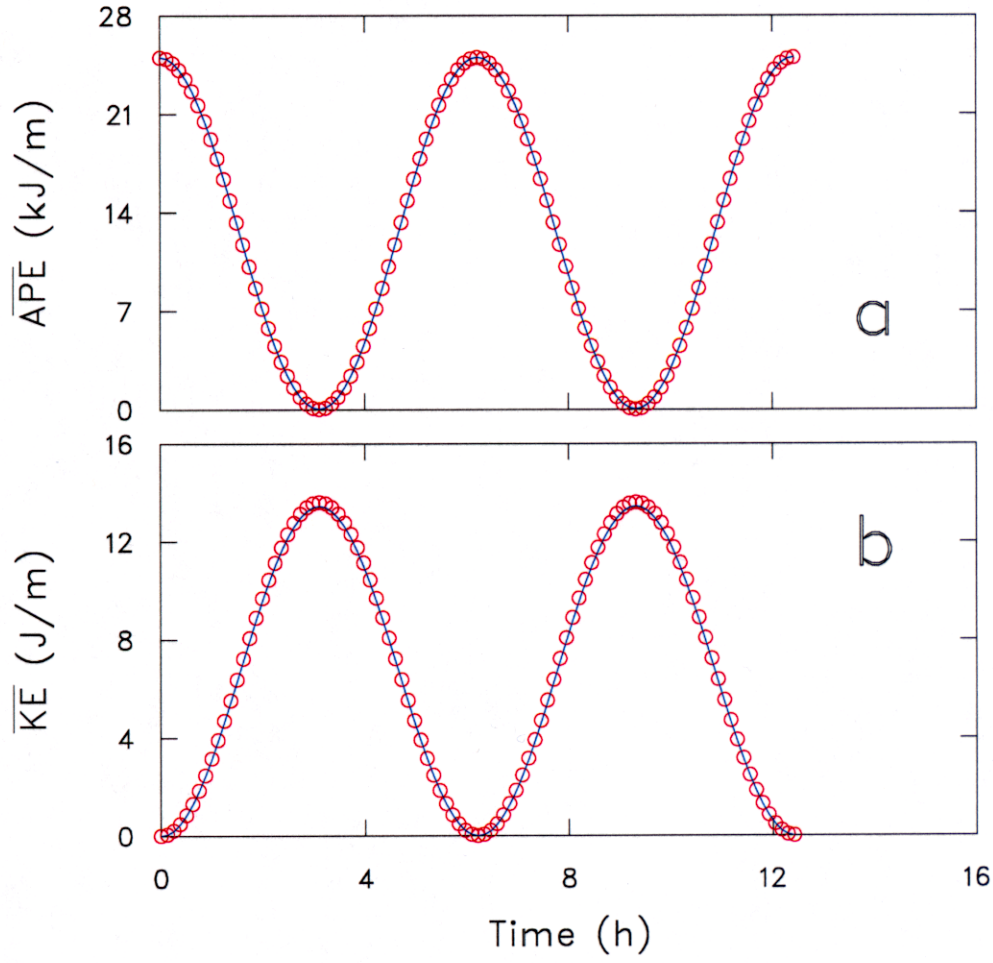

Figure 2: Barotropic energetics of analytical (solid blue line) and 128^2 grid numerical (red circles) solutions during one period of the M_2 tide: (a) available potential energy ($\overline{APE}$), in kilojoules/meter; and (b) kinetic energy ($\overline{KE}$), in Joules/meter.

analytical solution, and values of $\%d$ which are close to 100 indicate poor agreement of the model results with the analytical solution.

RESULTS

Visually, the comparison of the numerical to the analytical energetics for both the M_2 tidal period of the barotropic mode (Fig. 2) and for one period of the first baroclinic mode (Fig. 3) indicates excellent agreement between the energetics of the numerical results and those of the analytical solution.

The results of varying the spatial resolution of the numerical model, as summarized in Table 2 and Figs. 4–5, indicate rapid convergence to the analytical solution with increasing resolution. Both RMSE and $\%d$ decrease exponentially with increasing resolution for both the barotropic (Fig. 4) and baroclinic (Fig. 5) modes.

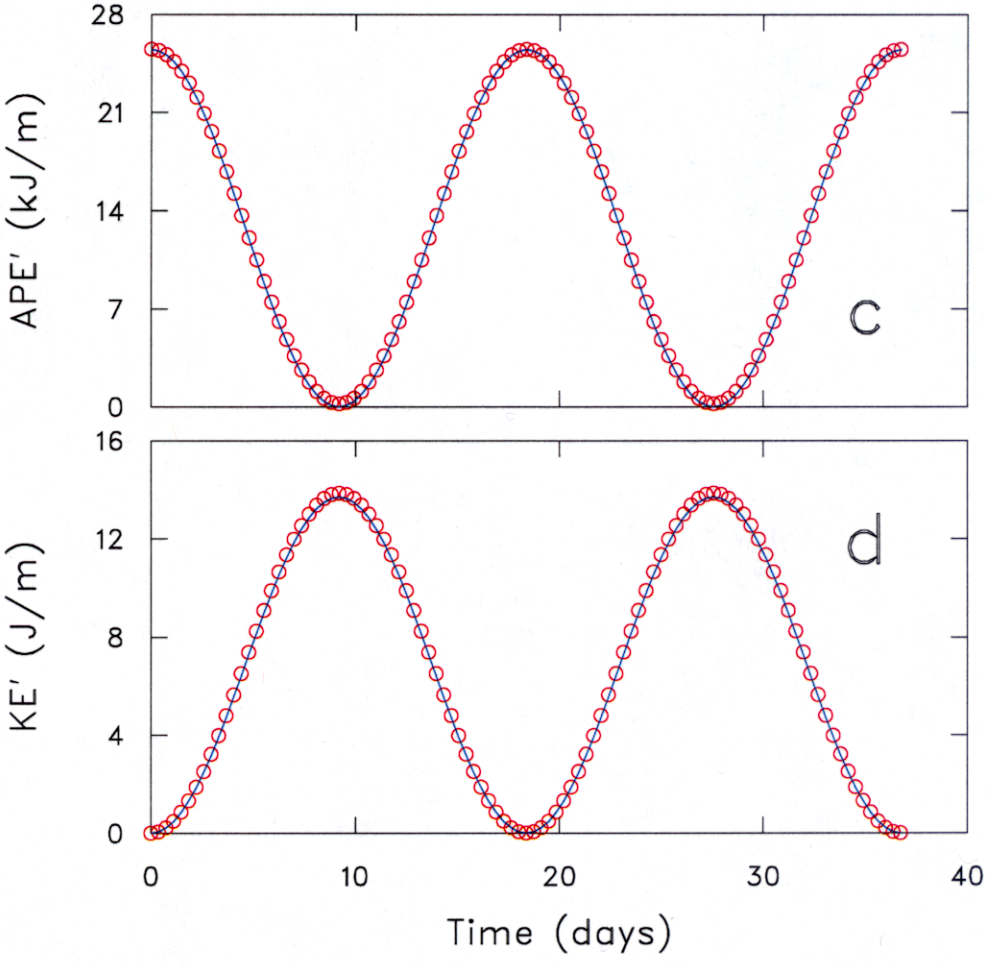

Figure 3: As for Fig. 2, except for baroclinic energetics during one period of the first baroclinc mode: (c) available potential energy (APE'), in kilojoules/meter; and (d) kinetic energy (KE'), in Joules/meter.

The low RMSE and $\%d$ results for $\overline{APE}$ indicate that the numerical model results for η agree better with the analytical results than those for $\bar{u}$ in the barotropic mode. Because the means over their corresponding period of the energetics of both the barotropic and baroclinic modes are very close (e.g., $< \overline{APE} > \approx < APE' > \approx 25\, rmk\, J$), their RMSE values may be compared. The fact that the barotropic mode results from the numerical model have lower RMSE and $\%d$ than the baroclinic results suggests that the barotropic results are more accurate than those of the baroclinic mode.Possible reasons for this disparity will be given in the Discussion section.

DISCUSSION

One possible reason for the disparity in the accuracy of the numerical model results from the barotropic versus baroclinic mode arises from the fact that the OBCs used in this study are local; i.e., dependent on the solution of the governing equations near the boundary (SLM99). As noted by SLM99, a local OBC in a primitive equation hydrostatic model such as that of the present study, "... is an ill-posed problem in that it is difficult to prove that a unique solution exists that is continuously dependent on boundary values." The use of the semi-implicit method for the barotropic mode propagates information from the open boundary back into the interior solution in the back-substitution portion of the Thomas algorithm, thus ensuring that the interior solution of the barotropic mode depends continuously on the boundary values. In contrast, the leapfrog solution method for the baroclinic mode does not allow for information propagation back into the interior from the open boundary.

Another possibility for the accuracy mismatch between the results of the barotropic and baroclinic modes of the numerical model also stems from the use of the semi-implicit method for the barotropic mode versus the leapfrog method for the baroclinic mode. For the barotropic OBC (Eq. 32), use of the semi-implicit method allows both η and $\bar{u}$ to be available at the $n+1$ time-level for use in the OBC (Eq. 36 in the Appendix). In contrast, for the baroclinic OBC (Eq. 33) only u' is available at the $n+1$ time-level using the leapfrog method, so p' for the OBC had to come from time-level n. Because Δt was decreased proportionally as resolution was increased (to keep the Courant number constant), the use of p'^n rather than p'^{n+1} for the OBC became a better and better approximation with increased spatial resolution, thereby contributing to the observed convergence. Convergence of the numerical baroclinic mode results to the analytical solution may thus be improved by an algorithm which allows both u'^{n+1} and p'^{n+1} to be present at that point in the solution when both are necessary for use in the u' OBC.

SUMMARY AND CONCLUSIONS

An analytical solution has been presented for the case of a stratified, tidally forced lagoon. The analytical solution is useful for the validation of numerical shallow water models under stratified conditions, especially the energetics of the solution. A simple finite-difference

Table 2: Root mean square error (RMSE) and percent disagreement, $\%d$, for the comparison of the model energetics results to the analytical solution for six different grid resolutions. The percent disagreement for $\overline{APE}$ has been multiplied by 10^9 for comparison purposes. * $\%d$ for $\overline{APE}$ from the 128^2 case == 0 (to 16 digits).

Grid	Quantity	RMSE (J/m)	$\%d$
128^2	$\overline{APE}$	1.25×10^{-4}	0.00*
	$\overline{KE}$	9.67×10^{-2}	1.02×10^{-2}
	APE'	1.21×10^{2}	4.57×10^{-3}
	KE'	9.86×10^{-2}	1.02×10^{-2}
64^2	$\overline{APE}$	5.02×10^{-4}	7.77×10^{-5}
	$\overline{KE}$	1.94×10^{-1}	4.06×10^{-2}
	APE'	2.42×10^{2}	1.83×10^{-2}
	KE'	1.98×10^{-1}	4.06×10^{-2}
32^2	$\overline{APE}$	2.01×10^{-3}	1.29×10^{-3}
	$\overline{KE}$	3.90×10^{-1}	1.60×10^{-1}
	APE'	4.81×10^{2}	7.34×10^{-2}
	KE'	3.97×10^{-1}	1.60×10^{-1}
16^2	$\overline{APE}$	8.03×10^{-3}	2.06×10^{-2}
	$\overline{KE}$	7.87×10^{-1}	6.23×10^{-1}
	APE'	9.55×10^{2}	3.00×10^{-1}
	KE'	8.03×10^{-1}	6.23×10^{-1}
8^2	$\overline{APE}$	3.21×10^{-2}	3.29×10^{-1}
	$\overline{KE}$	1.61	2.34
	APE'	1.91×10^{3}	1.30
	KE'	1.64	2.34
4^2	$\overline{APE}$	1.28×10^{-1}	5.26
	$\overline{KE}$	3.34	8.07
	APE'	3.94×10^{3}	6.60
	KE'	3.41	8.07

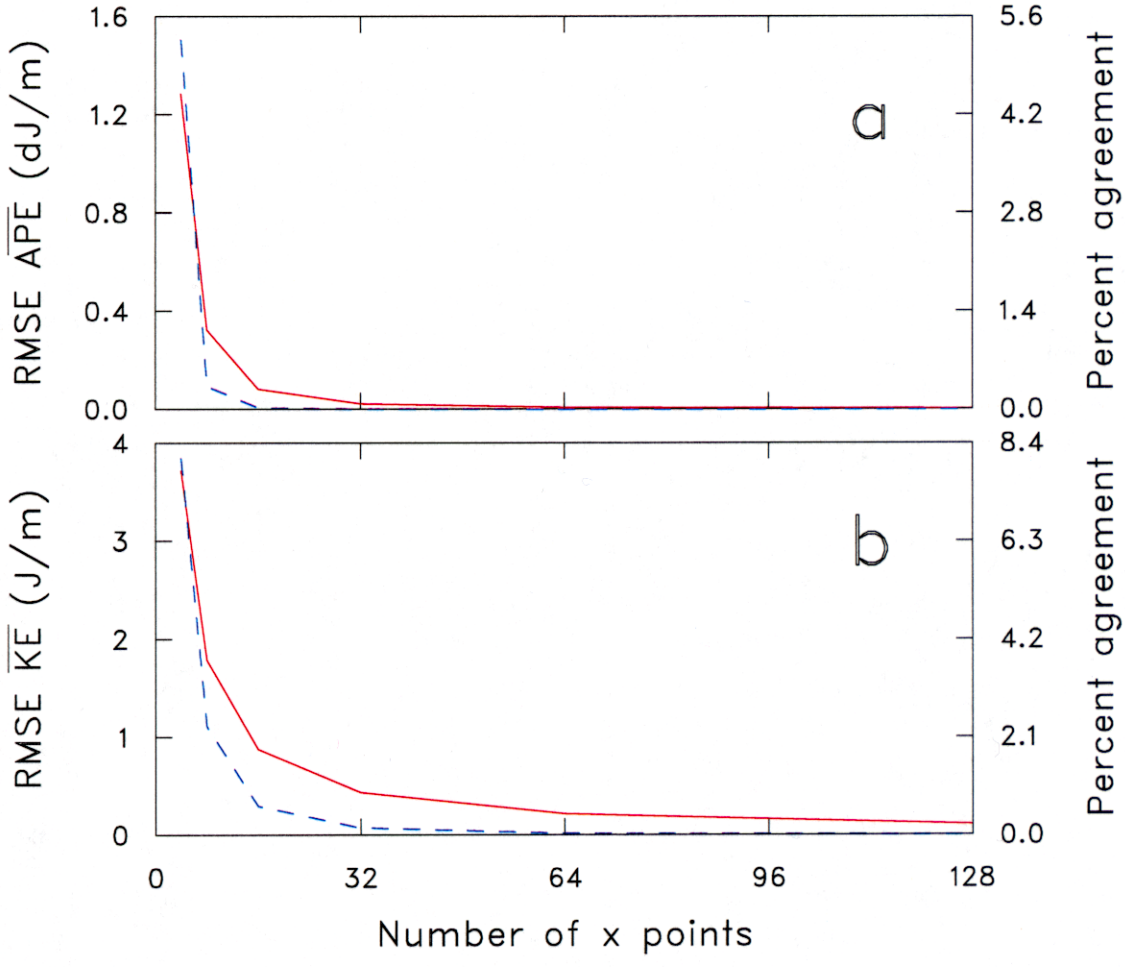

Figure 4: RMS error (RMSE, solid red line) and percent disagreement (dashed blue line) of the barotropic energetics of the numerical results with those of the analytical solution for several grid sizes (as number of density points in the x-direction: (a) available potential energy ($\overline{APE}$), and (b) kinetic energy ($\overline{KE}$). Note that RMSE for $\overline{APE}$ is in decijoules/meter, while RMSE for $\overline{KE}$ is in Joules/meter ($1\,J = 10\,dJ$); also, the percent disagreement for $\overline{APE}$ has been multiplied by 10^9.

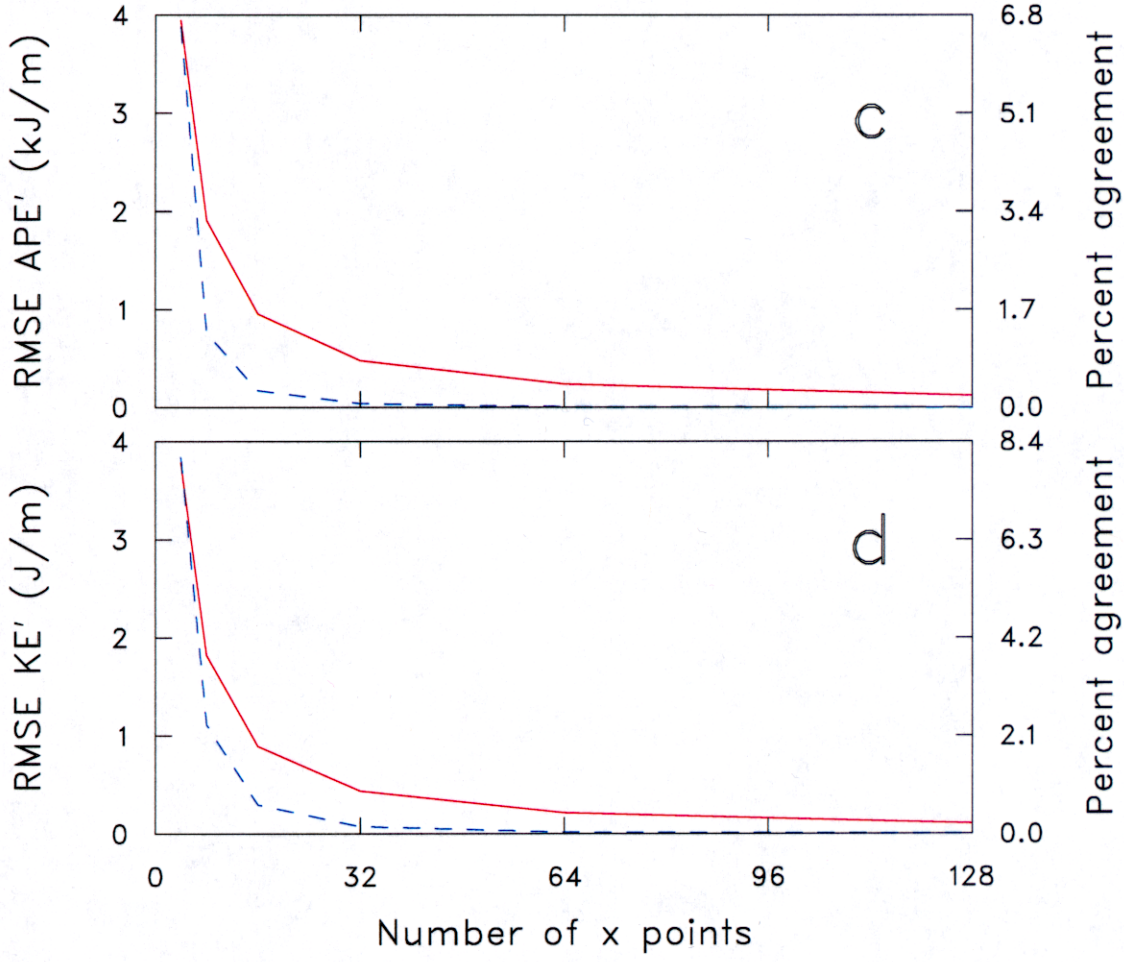

Figure 5: As for Fig. 4, except baroclinic rather than barotropic: (c) available potential energy (APE'), and (d) kinetic energy (KE'). Note that RMSE for APE' is in kilojoules/meter, while KE' is in Joules/meter.

model of the governing equations has been presented as an example of how the analytical solution can be used for such validation purposes. In particular, the comparison of the analytical and numerical solutions also of necessity involved the validation of the OBC employed by the numerical model.

The energetics results of the numerical model were shown to converge to those of the analytical model with increasing spatial resolution. This convergence validates both the numerical scheme employed (EB97) and also the OBC (an un-optimized version of SLM99). The slight mis-match between the convergence rates of the numerical results of the barotropic versus baroclinic modes to the analytical solution may be due either to the local nature of the leapfrog scheme of the baroclinic algorithm versus the global nature of the semi-implicit barotropic algorithm, or to the necessity of using a time-lagged pressure in the baroclinic OBC.

In conclusion, the analytical solution presented herein is a useful validation tool for numerical shallow water models in which both stratification and tidal forcing are important. Analytical solutions such as the present one should be used to validate numerical shallow water models for such simplified cases as this before such models are applied to the more realistic geophysical situations found in bays, harbors, and semi-enclosed seas.

ACKNOWLEDGEMENTS

This study was performed under the auspices of the U.S. Department of Energy by Lawrence Livermore National Laboratory under contract W-7405-ENG-48. This support is gratefully acknowledged.

REFERENCES

Eliason, D. E., and A. J. Bourgeois. 1997. Validation of numerical shallow water models for stratified seiches. *Int. J. Num. Meth. Fluids.* **24**: 771–786.

Flather, R. A. 1976. A tidal model of the northwest European continental shelf. *Mem. Soc. R. Sci. Liege*, Ser. 6. **10**: 141–164.

Livingston, G. P. 1981. Distribution of the crustacean zooplankton in a subtropical estuarine system: Implications for the predator-prey interaction between the primary and secondary consumers. Ph.D dissertation, Texas A&M University. 144 pp.

Reid, R. O., and B. R. Bodine. 1968. Numerical model for storm surges in Galveston Bay. *J. WaterwHarbors Coastal Eng. Div. Am. Soc. Civ. Eng.* **94**, 33–57.

Shulman, I., J. K. Lewis, and J. G. Mayer. 1999. Local data assimilation in the estimation of barotropic and baroclinic open boundary conditions. *J. Geophys. Res.* **104**: 13,667–13,680.

Thomas, L. H. 1949. Elliptic problems in linear difference equations over a network. Watson Sci. Comput. Lab. Rept. Columbia University, NY.

Thompson, K. W. 1987. Time dependent boundary conditions for hyperbolic systems. *J. Comp. Phys.* **68**: 1–24.

Wilmott, C. J. 1981. On the validation of models. *Phys. Geogr.* **2**: 184–194.

APPENDIX

A modification to the standard Thomas algorithm for solving the tridiagonal system of equations in the barotropic mode arises from the need to satisfy the OBC (Eq. 32) at $x = L$. The required modification involves computing the value of the solution vector at $i = I + 1$ such that it is consistent with both the OBC and the interior solution. The details of how this is done are presented in this appendix.

The Thomas algorithm first transforms the tridiagonal system of equations into one that is upper bidiagonal,

$$G_{2i} = E_{2i}G_{2i+1} + F_{2i}, \tag{35}$$

where G_{2i} is the solution vector, and E_{2i} and F_{2i} are the bidiagonal coefficients. In the forward sweep the E_{2i} and F_{2i} are computed from the tridiagonal coefficients. The boundary condition at $i = I + 1$ is then used to specify G_{2I+1} before back-substitution using Eq. 35. It is the specification of G_{2I+1} that must be made properly to implement the OBC. The method used in this study is to finite difference Eq. 32 and solve for $\eta_{I+1/2}$:

$$\eta^{n+1}_{I+1/2} = \frac{H}{c_0}(\bar{u}^{n+1}_{I+1} - \bar{u}^{n+1}_f) + \eta^{n+1}_f. \tag{36}$$

Expressing the bidiagonal equation in terms of $\bar{u}$ and η

$$\eta^{n+1}_{I+1/2} = E_{2I}\bar{u}^{n+1}_{I+1} + F_{2I}, \tag{37}$$

then elimininating $\eta^{n+1}_{I+1/2}$ from Eqs. 36–37 and solving for $\bar{u}^{n+1}_{I+1}$ gives

$$\bar{u}^{n+1}_{I+1} = \frac{H\bar{u}^{n+1}_f + c_0(F_{2I} - \eta^{n+1}_f)}{H - c_0E_{2I}}. \tag{38}$$

Identifying G_{2I+1} as $\bar{u}^{n+1}_{I+1}$, it is then set from the above expression to initialize the back-substitution phase of the Thomas algorithm.